Arabian Journal for Science and Engineering (2020) 45:9061–9073
https://doi.org/10.1007/s13369-020-04680-7

RESEARCH ARTICLE-MECHANICAL ENGINEERING

Mixed Convective Magneto Flow of SiO_2–MoS_2/$C_2H_6O_2$ Hybrid Nanoliquids Through a Vertical Stretching/Shrinking Wedge: Stability Analysis

Umair Khan[1] · **A. Zaib**[2] · **Fateh Mebarek-Oudina**[3]

Received: 30 January 2020 / Accepted: 29 May 2020 / Published online: 8 June 2020

Abstract

Hybrid nanoliquid as an expansion of nanoliquid is acquired by scattering combination of nano-powder or numerous distinct nanomaterials in the regular liquid. Hybrid nanofluids are impeding fluids which furnish better performance of heat transport and thermo-physical properties than convectional heat transport fluids (ethylene glycol, water and oil) and nanofluids with single material. At this juncture, a sort of hybrid nanofluid comprising nano-size materials through an ethylene glycol as a regular liquid is modeled to expand the magnetic impact on the mixed convection flow through a shrinking/stretched wedge. The impacts of Joule heating and viscous dissipation are also revealed. The PDEs which governed the flow problem with heat transport are changed into a dimensionless ODEs system through a similarity technique. Then these equations are numerically exercised by utilizing bvp4c solver. The impact of emerging constraints on the flow field with heat transport is discussed with the aid of plots. Also, the stability analysis is implemented to classify which result is physically reliable and stable.

Keywords Hybrid nanoliquid · Mixed convection · Stretched/shrinking wedge · Stability

List of Symbols

U_0, U_∞	Constants
B_0	Magnetic field strength
C_F	Skin friction coefficient
c_p	Specific heat
Ec	Eckert number
f	Dimensionless velocity
g	Gravity acceleration
Gr_x	Grashof number
k	Thermal conductivity
M	Magnetic number
m	Falkner–Skan power-law parameter
Nu_x	Nusselt number
Pr	Prandtl number
Re_x	Local Reynolds number
s	Suction parameter
T	Temperature
$T_w(x)$	Wall temperature
T_∞	Ambient temperature
θ	Dimensionless temperature
(u, v)	Velocity components
$u_w(x)$	Stretching velocity
$u_\infty(x)$	Free stream velocity
v_w	Mass flux velocity
(x, y)	Cartesian coordinates

Greek Symbols

α	Thermal diffusivity
β	Thermal expansion
β_1	Hartree of pressure
ε	Wall thickness parameter
λ	Stretching/shrinking parameter
λ_1	Mixed convection parameter
ς	Growth and decay distribution parameter
μ	Dynamic viscosity
Ω	Angle
ϕ_1, ϕ_2	The volume fraction of nanoparticles
ν_f	Kinematic viscosity of the base fluid
ρ	Density
σ	The electrical conductivity

✉ Fateh Mebarek-Oudina
f.mebarek_oudina@univ-skikda.dz; oudina2003@yahoo.fr

[1] Department of Mathematics and Social Sciences, Sukkur IBA University, Sukkur 65200, Sindh, Pakistan

[2] Department of Mathematical Sciences, Federal Urdu University of Arts, Science and Technology, Gulshan-E-Iqbal, Karachi 75300, Pakistan

[3] Department of Physics, Faculty of Sciences, University of 20 août 1955-Skikda, Road El-Hadaiek, B.P. 26, 21000 Skikda, Algeria

τ	Dimensionless variable
(ρc_p)	Heat capacity
ψ	Stream function
η	Similarity variable

Subscripts

f	Base fluid
s_1,s_2	Solid nanoparticles
nf	Nanofluid
hnf	Hybrid nanofluid
w	Wall boundary condition
∞	Free-stream condition

Superscripts

ʻ	Derivative w.r.t. η

1 Introduction

In the current era, nanoliquids are renowned smartly engineer liquids completed of a regular liquid and nanomaterials (1.00–100.00 nm). Such kinds of liquids have superior thermal conductivity and heat transport coefficients of single phase as compared to conventional liquids. A novel type of nanoliquid be constructed by mixing two distinct types of nanomaterials named nano-composite or hybrid particles in the regular liquid, is known hybrid or nano-composite liquid. The hybrid nanomaterial is a material which merges chemical and physical characteristics of distinct nanomaterials simultaneously and offers the homogenous phase properties. These given hybrid nanoliquids are realistically a novel class of nanoliquids which has several imaginable applications in entirely heat transport fields, e.g. acoustics, manufacturing, defense, micro fluidics, transportation, naval structures, etc. Improvement of hybrid nanoliquids with superiority stability and thermal conductivity augmented is significant and can guide to optimization and sustainability of energy, since it enhances the thermal system efficiency [1]. Sarkar et al. [2] and Sidik et al. [3] have précised the earlier and current research and improvement correlated to preparation techniques of hybrid nanoliquids, the properties of thermophysical of hybrid nanoliquids and recent applications of hybrid nanoliquids. Senthilraja et al. [4] experimentally scrutinized water based Al_2O_3/CuO nanoparticles and Al_2O_3-CuO hybrid nanoliquid. Toghraiel et al. [5] explored the thermal properties of ethylene glycol based ZnO-TiO_2 hybrid nanoliquid and the temperature fluctuated from 25 to 50 °C and volume fraction particle from 0 to 3.5%. Also, it was monitored that at a lower temperature enhancement of thermal conductivity was less contrasted to a higher temperature. The impact of water based hybrid nanoliquid through mixing nanoparticles (TiO_2, SiO_2 and Al_2O_3) with distinct viscosity was estimated by Adriana et al. [6]. Maraj et al. [7] scrutinized the influence of shape factor by utilizing the carrying of hybrid MoS_2–SiO_2/H_2O nanoparticles through an isothermal porous vertical cone. They also considered the viscous dissipation and magnetic impacts. Rostami et al. [8] scrutinized the influence of magnetic field on forced and free convection flow of hybrid SiO_2–Al_2O_3–H_2O nanofluids from a porous vertical surface. The nonlinear radiative time dependent flow water based Cu-Al_2O_3 hybrid micropolar nanofluid suspended in polar materials was explored by Mackolil and Mahanthesh [9]. The data of linear regression for the friction factor and Nusselt number are also analyzed. Shruthy and Mahanthesh [10] investigated Casson liquid containing hybrid nanoliquid with thermal Rayleigh–Bénard convection and obtained the analytic solution. They observed that the hybrid nanoliquid stoppages the convection. Ghadikolaei et al. [11] explored the 3D magneto impact on the free convective flow comprising hybrid MoS_2-Ag nanomaterials mixed in water based $C_2H_6O_2$ nanoparticle with radiation effect. Mackolil and Mahanthesh [12] inspected the impact of heat absorption on the radiative flow of Casson nanofluid with diffusion-thermo effect and applied sensitivity analysis to obtain the solution. The impact of magnetic function on the flow of hybrid nanoliquid suspended in water and ethylene glycol base fluid was examined Mahanthesh [13]. Ashlin and Mahanthesh [14] investigated water based alumina nanofluid as well as copper/alumina hybrid nanoliquid through a vertical plate owing to co-axial rotation with five different shapes. They utilized the Laplace technique to find the exact solution. Recently, Thriveni and Mahanthesh [15] applied the sensitivity analysis to study the magneto radiative flow of hybrid nanoliquid with mixed convective.

Owing to applications of shrinking and stretching sheets in the majority of the modern techniques, researchers have been eager to investigate the flows containing shrinking/stretching sheets. These include heating or cooling of films, polymer processes, conveyor belts, insulating materials, etc. From the family of the boundary-layer flow, Falkner and Skan [16] discovered the similarity results of flow through a stationary wedge. Hartree [17], Koh and Hartnett [18] implemented the boundary-layer assumptions to investigate the flow problem through a wedge by taking different engaged factors. Postelnicu and Pop [19] discussed the Falker–Skan flow comprising power law liquid from a stretched wedge. They found the multiple solutions for some fixed value of m, n and f_0. The impacts of magnetic and radiation parameters on forced and free convective 2D flow with heat transport from a stretched porous wedge with Joule heating were scrutinized by Su et al. [20] and obtained the solutions using an innovative technique named as DTM-BF. Yang and Machado [21] addressed the operator of new fractional-order of the erratic order first time and also presented the Fourier and Laplace transforms. The impact of bio-convection flow of a nanoliquid involving microorganism from a fixed wedge in a Darcy medium is studied by Zaib et al. [22]. Yang [23] reported the new results of the general fractional calculus and also proposed new special functions. Yang and Gao [24] proposed Sumudu transform to solve the heat and diffusion equations. Yang [25] addressed the fractional derivatives of variables as well as of constant orders applied in different kinds of the problems in heat transfer. He applies the derivative in the form of Caputo type derivative. Yang and coauthors [26–28] suggested the fundamental results of the anomalous and general fractional order diffusion equation with singular, negative Prabhakar, non-singular and exponential decay kernels. The impact of the induced magnetic field of steady 2D flow containing nanofluid through a moving as well as fixed wedge was monitored by Nadeem et al. [29]. Recently, various studies on nanofluids are carried out in refs.[30–35].

The foregoing literature review discloses that the general problem of mixed convection containing hybrid nanofluids particularly stretching/shrinking wedge with Joule heating and dissipation has been underlined as mostly unexplored fields. Thus, the current work aims to scrutinize the hybrid nanoliquid magneto flow through a shrinking/stretching wedge with mixed convection by utilizing the mathematical model of hybrid nanoliquids suggested by the Devi and Devi [36], and Hayat and Nadeem [37]. In addition, the Joule heating and viscous dissipation impacts are also captivating. Here, hybrid nanoliquid is formed by mixing two distinct nanoparticles that are SiO_2 (silicon dioxide) and MoS_2 (Molybdenum disulfide) in the regular liquid (ethylene glycol). MoS_2 has a structure in layered form and it is utilized as a catalyst and lubricant due to its distinctive properties like chemical inertness, anisotropy and resistance of photo corrosion. In addition, MoS_2 nanomaterials product may be employed as nanocatalyses hydrogenation. The leading PDEs are transmuting into nonlinear ODEs through an appropriate transformation and then these ODEs are tackled via bvp4c. Influences of the pertinent constraints are investigated and portrayed via the plots.

2 Problem Statement

Consider the 2D steady mixed convective flow with heat transport containing hybrid nanoparticles through a porous wedge as portrayed in Fig. 1. The viscous dissipation with Joule heating also invoked here. The ethylene glycol based SiO_2–MoS_2 nanoparticles have been taken in this investigation. In this model, initially SiO_2 scattered into the regular liquid (ethylene glycol), and then to develop the marked hybrid nanoliquid SiO_2–MoS_2/$C_2H_6O_2$, MoS_2 is diffused in nanoliquid SiO_2/ethylene glycol. In extra assumption, the variable magnetic field is applied normal to wedge walls. It is supposed that moving wedge and the ambient velocity flow are respectively $u_w(x)$ and $u_\infty(x)$, whereas the walls temperature and the ambient temperature are respectively, $T_{\mathrm{w}}(x)$ and T_∞ with $T_{\mathrm{w}}(x) > T_\infty$ utilized for the assisting flow (heated surface) and $T_{\mathrm{w}}(x) < T_\infty$ consumed for the opposing flow (cooled surface). Applying the Boussinesq with boundary layer approximations, the steady leading equations are

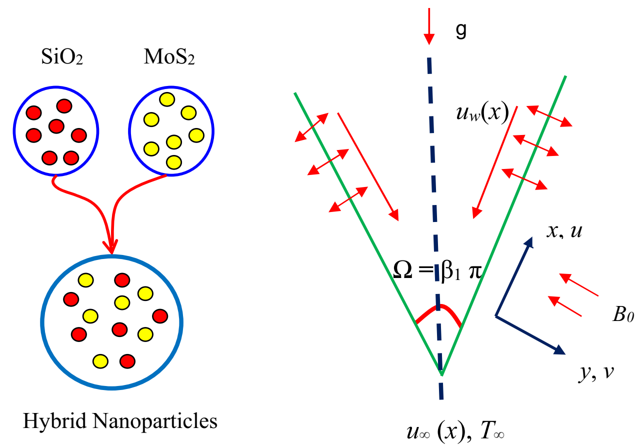

Fig. 1 Physical diagram of the problem

$$\frac{\partial v}{\partial y} + \frac{\partial u}{\partial x} = 0, \tag{1}$$

$$u\frac{\partial u}{\partial x} + v\frac{\partial u}{\partial y} = u_\infty \frac{du_\infty}{dx} + \frac{\mu_{\mathrm{hbnf}}}{\rho_{\mathrm{hbnf}}}\frac{\partial^2 u}{\partial y^2} + \frac{\sigma_{\mathrm{hbnf}}B^2(x)}{\rho_{\mathrm{hbnf}}}\left(u_\infty - u\right) + \frac{g(\rho\beta)_{\mathrm{hbnf}}}{\rho_{\mathrm{hbnf}}}\left(T - T_\infty\right)\cos\left(\frac{\Omega}{2}\right), \tag{2}$$

$$u\frac{\partial T}{\partial x} + v\frac{\partial T}{\partial y} = \frac{k_{\mathrm{hbnf}}}{\left(\rho c_{\mathrm{p}}\right)_{\mathrm{hbnf}}}\frac{\partial^2 T}{\partial y^2} + \frac{\sigma_{\mathrm{hbnf}}B^2(x)}{\left(\rho c_p\right)_{\mathrm{hbnf}}}u^2 + \frac{\mu_{\mathrm{hbnf}}}{\left(\rho c_{\mathrm{p}}\right)_{\mathrm{hbnf}}}\left(\frac{\partial u}{\partial y}\right)^2. \tag{3}$$

The physical boundary conditions are

$$\begin{aligned} &u = u_{\mathrm{w}}(x),\ v = v_{\mathrm{w}}, T = T_{\mathrm{w}}(x) \text{ at } y = 0, \\ &u = u_\infty(x),\ T \to T_\infty \text{ as } y \to \infty, \end{aligned} \tag{4}$$

in which v and u are components of velocity respectively in $y-$ and x-directions. Moreover, these symbols $\rho_{\mathrm{hbnf}}, \mu_{\mathrm{hbnf}}, \sigma_{\mathrm{hbnf}}, g, (\rho\beta)_{\mathrm{hbnf}}, v_{\mathrm{w}}$ are called density, dynamic viscosity, electrical conductivity, gravitational acceleration, coefficient of thermal expansion, suction of hybrid nanoliquids, respectively.

2.1 Thermophysical Properties of Hybrid Nanofluid

The combination of hybrid nanoliquid comprising $SiO_2\left(\phi_1\right)$ and $MoS_2\left(\phi_2\right)$ nanoparticles in ethylene glycol considered as a regular liquid. Furthermore, volume fractions of nanoparticle SiO_2 has been set to 1% and of MoS_2 vary from 1 to 5%. Following Xie et al. [38], the volume fraction of hybrid nanoliquid is suggested as

$$\phi_{\mathrm{hnf}} = \frac{V_{\mathrm{SiO_2}} + V_{\mathrm{MoS_2}}}{V_{\mathrm{Total}}} = \phi_1 + \phi_2.$$

Moreover, Table 1 is prepared to show the thermophysical attributes of the hybrid nanoliquid.

Following Deswita et al. [39]; Ishak et al. [40], the values of $u_{\mathrm{w}}(x)$,$u_\infty(x)$, $T_{\mathrm{w}}(x)$ and $B(x)$ are invoked in the text are given below as

$$u_{\mathrm{w}}(x) = U_0 x^m, u_\infty(x) = U_\infty x^m, T_{\mathrm{w}}(x) - bx^{(5m-1)/2} = T_\infty, B(x) = B_0 x^{\frac{m-1}{2}}, \tag{5}$$

where U_0, U_∞ are constant velocities and $m = \frac{-\beta_1}{(\beta_1-2)}$ with β_1 is called the parameter named as Hartree of pressure slope which joins to $\beta_1 = \Omega/\pi$ for a wedge material angle, B_0 called the strength of magnetic.

One would take the following similarity variables:

$$u = u_\infty(x)F'(\eta),\ v = -\left(\frac{(1+m)\nu_{\mathrm{f}} u_\infty(x)}{2x}\right)^{\frac{1}{2}}\left[F(\eta) + \left(\frac{m-1}{m+1}\right)\eta F'(\eta)\right],$$
$$\eta = y\left(\frac{(1+m)u_\infty(x)}{2\nu_f x}\right)^{\frac{1}{2}},\ \theta(\eta)\left(T_{\mathrm{w}} - T_\infty\right) + T_\infty = T. \tag{6}$$

Implementation of the transformations above into Eqs. (2)–(5) and to get consistent transmuted ODEs via the well-known equation (6) become as

$$F'''X_1^{-1} + X_2\left(\frac{2m}{m+1}\left(1 - (F')^2\right) + FF''\right) + \left(\frac{2}{m+1}\right)MX_3(1 - F') + \left(\frac{2}{m+1}\right)\lambda_1 \cos\left(\frac{\Omega}{2}\right)X_4\theta = 0, \tag{7}$$

$$X_5\theta'' + \Pr X_6\left(F\theta' - \left(\frac{5m-1}{m+1}\right)\theta F'\right) + \Pr EcM\left(\frac{2}{m+1}\right)F'^2 + \frac{\Pr Ec}{X_1}\left(F''\right)^2 = 0, \tag{8}$$

with the dimensional form of boundary restriction is

$$F(0) - s = 0, F'(0) - \lambda = 0, \theta(0) - 1 = 0,$$
$$F'(\infty) - 1 \to 0, \theta(\infty) \to 0, \tag{9}$$

in which

$$X_1 = \left(1-\phi_1\right)^{2.5}\left(1-\phi_2\right)^{2.5},$$
$$X_2 = \left(\left(1-\phi_2\right)\left\{\left(1-\phi_1\right) + \phi_1\frac{\rho_{s_1}}{\rho_{\mathrm{f}}}\right\} + \phi_2\frac{\rho_{s_2}}{\rho_{\mathrm{f}}}\right),$$
$$X_3 = \left(\frac{\sigma_{s_2}\left(1+2\phi_2\right) + 2\sigma_{\mathrm{bf}}\left(1-\phi_2\right)}{\sigma_{s_2}\left(1-\phi_2\right) + \sigma_{\mathrm{bf}}\left(2+\phi_2\right)}\right)\left(\frac{\sigma_{s_1}\left(1+2\phi_1\right) + 2\sigma_{\mathrm{f}}\left(1-\phi_1\right)}{\sigma_{s_1}\left(1-\phi_1\right) + \sigma_{\mathrm{f}}\left(2+\phi_1\right)}\right),$$
$$X_4 = \left(\left(1-\phi_2\right)\left[\left(1-\phi_1\right) + \phi_1\frac{(\rho\beta)_{s_1}}{(\rho\beta)_{\mathrm{f}}}\right] + \phi_2\frac{(\rho\beta)_{s_2}}{(\rho\beta)_{\mathrm{f}}}\right),$$
$$X_5 = \left[\left(\frac{k_{s_2} + 2k_{\mathrm{nf}} - 2\phi_2\left(k_{\mathrm{nf}} - k_{s_2}\right)}{k_{s_2} + 2k_{\mathrm{nf}} + \phi_2\left(k_{\mathrm{nf}} - k_{s_2}\right)}\right)\left(\frac{\left(k_{s_1} + 2k_{\mathrm{f}}\right) - 2\phi_1\left(k_{\mathrm{f}} - k_{s_1}\right)}{\left(k_{s_1} + 2k_{\mathrm{f}}\right) + \phi_1\left(k_{\mathrm{f}} - k_{s_1}\right)}\right)\right],$$
$$X_6 = \left(\left(1-\phi_2\right)\left[\left(1-\phi_1\right) + \phi_1\frac{\left(\rho c_{\mathrm{p}}\right)_{s_1}}{\left(\rho c_{\mathrm{p}}\right)_{\mathrm{f}}}\right] + \phi_2\frac{\left(\rho c_{\mathrm{p}}\right)_{s_2}}{\left(\rho c_{\mathrm{p}}\right)_{\mathrm{f}}}\right). \tag{9A}$$

The non-dimensional patent parameters in Eqs. (7) and (8) which are expressed as mathematically

Table 1 Thermophysical characteristics of hybrid nanofluid

Properties	Hybrid nanofluid
Density	$\rho_{\mathrm{hbnf}} = \rho_{\mathrm{f}}\left[\left(1-\phi_2\right)\left\{\left(1-\phi_1\right) + \phi_1\left(\frac{\rho_{s_1}}{\rho_{s_1}}\right)\right\} + \phi_2\left(\frac{\rho_{s_2}}{\rho_{s_1}}\right)\right]$
Viscosity	$\mu_{\mathrm{hbnf}} = \mu_f\left(1-\phi_1\right)^{-2.5}\left(1-\phi_2\right)^{-2.5}$
Thermal expansion	$(\rho\beta)_{\mathrm{hbnf}} = (\rho\beta)_{\mathrm{f}}\left(\left(1-\phi_2\right)\left[\left(1-\phi_1\right) + \phi_1\left(\frac{(\rho\beta)_{s_1}}{(\rho\beta)_{\mathrm{f}}}\right)\right] + \phi_2\left(\frac{(\rho\beta)_{s_2}}{(\rho\beta)_{\mathrm{f}}}\right)\right)$
Electrical conductivity	$\sigma_{\mathrm{hbnf}} = \sigma_{\mathrm{bf}}\left[\frac{\sigma_{s_2}(1+2\phi_2)+2\sigma_{\mathrm{bf}}(1-\phi_2)}{\sigma_{s_2}(1-\phi_2)+\sigma_{\mathrm{bf}}(2+\phi_2)}\right]$ with $\sigma_{\mathrm{bf}} = \sigma_{\mathrm{f}}\left[\frac{\sigma_{s_1}(1+2\phi_1)+2\sigma_{\mathrm{f}}(1-\phi_1)}{\sigma_{s_1}(1-\phi_1)+\sigma_{\mathrm{f}}(2+\phi_1)}\right]$
Thermal conductivity	$\frac{k_{\mathrm{hbnf}}}{k_{\mathrm{nf}}} = \frac{\left(k_{s_2}+2k_{\mathrm{nf}}\right)-2\phi_2\left(k_{\mathrm{nf}}-k_{s_2}\right)}{\left(k_{s_2}+2\hat{k}_{\mathrm{nf}}\right)+\phi_2\left(\hat{k}_{\mathrm{nf}}-\hat{k}_{s_2}\right)}$ with $k_{\mathrm{nf}} = \frac{1-2\phi_1\left(\frac{\left(k_{\mathrm{f}}-k_{s_1}\right)}{\left(k_{s_1}+2k_{\mathrm{f}}\right)}\right)}{1+\phi_1\left(\frac{\left(k_{\mathrm{f}}-k_{s_1}\right)}{\left(k_{s_1}+2k_{\mathrm{f}}\right)}\right)} \times k_{\mathrm{f}}$
Heat capacity	$\left(\rho c_{\mathrm{p}}\right)_{\mathrm{hbnf}} = \left(\rho c_{\mathrm{p}}\right)_{\mathrm{f}}\left(\left(1-\phi_2\right)\left[\left(1-\phi_1\right) + \phi_1\left(\frac{\left(\rho c_{\mathrm{p}}\right)_{s_1}}{\left(\rho c_{\mathrm{p}}\right)_{\mathrm{f}}}\right)\right] + \phi_2\left(\frac{\left(\rho c_{\mathrm{p}}\right)_{s_2}}{\left(\rho c_{\mathrm{p}}\right)_{\mathrm{f}}}\right)\right)$

$$\lambda_1 = \frac{\mathrm{Gr}_x}{\mathrm{Re}_x^2}, M = \frac{\sigma_f B_0^2}{\rho_f U_\infty}, \mathrm{Re}_x = \frac{x u_\infty(x)}{\nu_f},$$
$$\mathrm{Pr} = \frac{\nu_f}{\alpha_f}, \mathrm{Gr}_x = \frac{g\beta_f\left(T_w - T_\infty\right)x^3}{\nu_f^2},$$
$$\lambda = \frac{U_w}{U_\infty}, \mathrm{Ec} = \frac{u_\infty^2}{\left(c_p\right)_f\left(T_w - T_\infty\right)}. \tag{9B}$$

While these parameters namely called the mixed convective parameter $\left(\lambda_1\right)$ (where it is defined as $\lambda_1 = \frac{\mathrm{Gr}_x}{\mathrm{Re}_x^2}$ called the fraction of $\left(\mathrm{Gr}_x\right)$ Grashof number and the Reynolds number $\left(\mathrm{Re}_x\right)$, magnetic parameter ($M$), Prandtl number (Pr), Eckert number (Ec) and the stretching/ shrinking parameter (λ), respectively.

3 Numerical Process

There are several techniques for solving nonlinear problems such as [41–46]. Prior utilizing the bvp4c solver based on 3-stage Lobatto technique which is handy to hold the 1st-order initial value problem. In general, Lobatto IIIA techniques have been used for the BVP owing to their extremely excellent properties of stability and contain accuracy of fourth-order over the entire interval. First the leading differential equations are transmuted into the first order group of ODEs. To achieve this, assume the new variables:

$$F = R_1^*, F' = R_2^*, F'' = R_3^*, \theta = R_4^*, \theta' = R_5^*. \tag{14}$$

The dependent first-order system is obtained as

$$\begin{pmatrix} R_1^{*\prime} \\ R_2^{*\prime} \\ R_3^{*\prime} \\ R_4^{*\prime} \\ R_5^{*\prime} \end{pmatrix} = \begin{pmatrix} R_2^* \\ R_3^* \\ -\mathrm{X}_1\mathrm{X}_2\left(R_1^*R_3^* + \frac{2m}{m+1}\left(1-\left(R_2^*\right)^2\right)\right) - \mathrm{X}_1\mathrm{X}_3 M\left(\frac{2}{m+1}\left(1-R_2^*\right)\right) - \\ \mathrm{X}_1\mathrm{X}_4\lambda_1\left(\frac{2}{m+1}\cos\left(\frac{\Omega}{2}\right)R_4^*\right) \\ R_5^* \\ \dfrac{\left(-M\,\mathrm{Pr}\,Ec\left(\frac{2}{m+1}\left(R_2^*\right)^2\right) - \mathrm{Pr}\,\mathrm{X}_6\left(R_1^*R_5^* - \left(\frac{5m-1}{m+1}\right)R_2^*R_4^*\right) - \frac{\mathrm{Pr}\,\mathrm{Ec}\left(R_3^*\right)^2}{\mathrm{X}_1}\right)}{\mathrm{X}_5} \end{pmatrix}, \tag{15}$$

The local rate of heat transfer (Nusselt number) and the skin friction factor are the physical significant quantities concerning on the flow with heat transport. These quantities in the ODEs form are

$$Nu_x = \frac{-k_{hbnf}x}{k_f\left(T_w - T_\infty\right)}\left(\frac{\partial T}{\partial y}\right)_{y=0}, \tag{10}$$

$$C_F = \frac{\mu_{hbnf}}{\rho u_\infty^2(x)}\left(\frac{\partial u}{\partial y}\right)_{y=0}. \tag{11}$$

Applying (6), we get

$$\left(\mathrm{Re}_x\right)^{\frac{-1}{2}}\mathrm{Nu}_x = \frac{-k_{hbnf}\theta'(0)}{k_f}\left\{\frac{m+1}{2}\right\}^{\frac{1}{2}}, \tag{12}$$

$$\sqrt{\mathrm{Re}_x}C_F = \frac{F''(0)}{\left(1-\phi_1\right)^{2.5}\left(1-\phi_2\right)^{2.5}}\left\{\frac{m+1}{2}\right\}^{\frac{1}{2}}. \tag{13}$$

and the reformed initial conditions are

$$\begin{pmatrix} R_1^*(0) \\ R_2^*(0) \\ R_2^*(\infty) \\ R_4^*(0) \\ R_4^*(\infty) \end{pmatrix} = \begin{pmatrix} s \\ \lambda \\ 1 \\ 1 \\ 0 \end{pmatrix}. \tag{16}$$

Throughout this exploration, the set of up non-linear ODEs is numerically attempted by utilizing the bvp4c solver. The above problem may possibly have dual results; thus the assumed numerical method needs distinct early guesses to accomplish the conditions (9). In addition, the early value is relatively easy and simple to obtain the first solution (FS). Meanwhile, it is relatively difficult to obtain the precise initial guess for the second solution (SS). The numerical integration range is taken to be $\eta_{\max} = 3$ in the computation that is sufficient for the graphical outcomes to accomplish the two point condition asymptotically. The size of step is taken as $\Delta\eta = \frac{1}{100}$. The iteratively procedure is replicated awaiting the obligatory results are achieved up to accuracy level 10^{-5} to fit the convergence criterion.

4 Stability Analysis of the Solution

When one does the stability analysis, it is done with the primary objective to obtain the result of the aforementioned problem to check that the physical realization of the first branches in practice and to what extent and as well as for the (SS) that is not physically realizable. The unsteady equation would be taken in a specific order to determine their physical significance is given as under

$$\frac{\partial v}{\partial y}+\frac{\partial u}{\partial x}=0, \tag{17}$$

$$\frac{\partial u}{\partial t}+u\frac{\partial u}{\partial x}+v\frac{\partial u}{\partial y}=u_\infty\frac{du_\infty}{dx}+\frac{\mu_{\text{hbnf}}}{\rho_{\text{hbnf}}}\frac{\partial^2 u}{\partial y^2}+\frac{\sigma_{\text{hbnf}}B^2(x)}{\rho_{\text{hbnf}}}\left(u_\infty-u\right)+\frac{g(\rho\beta)_{\text{hbnf}}}{\rho_{\text{hbnf}}}\left(T-T_\infty\right)\cos\left(\frac{\Omega}{2}\right), \tag{18}$$

$$\frac{\partial T}{\partial t}+u\frac{\partial T}{\partial x}+v\frac{\partial T}{\partial y}=\frac{k_{\text{hbnf}}}{\left(\rho c_p\right)_{\text{hbnf}}}\frac{\partial^2 T}{\partial y^2}+\frac{\sigma_{\text{hbnf}}B^2(x)}{\left(\rho c_p\right)_{\text{hbnf}}}u^2+\frac{\mu_{\text{hbnf}}}{\left(\rho c_p\right)_{\text{hbnf}}}\left(\frac{\partial u}{\partial y}\right)^2. \tag{19}$$

Aforementioned model of stability, declare the fresh time variable that is dimensionless τ. For this stability model the similarity transformation has now become as

$$\begin{aligned}
&u=U_\infty x^m F'(\eta),\\
&v=-\sqrt{\frac{(1+m)v_{\text{f}}U_\infty}{2}}x^{\frac{m-1}{2}}\left[\left(\frac{m-1}{m+1}\right)\eta F'(\eta)+F(\eta)\right],\\
&\eta=y\sqrt{\frac{(1+m)U_\infty}{2v_{\text{f}}}}x^{\frac{m-1}{2}},\ \theta(\eta)\left(T_{\text{w}}-T_\infty\right)+T_\infty=T,\\
&\tau=\frac{\text{m}\ +\ 1}{2}\left(\frac{u_\infty(x)}{x}\right)t.
\end{aligned} \tag{20}$$

By plugging Eq. (20) into Eqs. (18) and (19), we get

$$\frac{\partial^3 F}{\partial\eta^3}\text{X}_1^{-1}+\text{X}_2\left(F\frac{\partial^2 F}{\partial\eta^2}+\frac{2m}{m+1}\left(1-\left(\frac{\partial F}{\partial\eta}\right)^2\right)-\frac{\partial^2 F}{\partial\eta\partial\tau}\right)+\left(\frac{2}{m+1}\right)M\text{X}_3\left(1-\frac{\partial F}{\partial\eta}\right)+\left(\frac{2}{m+1}\right)\lambda_1\cos\left(\frac{\Omega}{2}\right)\text{X}_4\theta=0 \tag{21}$$

$$\frac{\partial^2\theta}{\partial\eta^2}\text{X}_5+\Pr\text{Ec}M\left(\frac{2}{m+1}\right)\left(\frac{\partial F}{\partial\eta}\right)^2+\Pr\text{X}_6\left(F\frac{\partial\theta}{\partial\eta}-\left(\frac{5m-1}{m+1}\right)\theta\frac{\partial F}{\partial\eta}-\frac{\partial\theta}{\partial\tau}\right)+\frac{\Pr\text{Ec}}{\text{X}_1}\left(\frac{\partial^2 F}{\partial\eta^2}\right)^2=0, \tag{22}$$

and the subjected conditions are

$$\begin{aligned}
&F(0,\tau)=s,\ \frac{\partial F(0,\tau)}{\partial\eta}=\lambda,\ \theta(0,\tau)=1,\ \text{at}\ \eta=0\\
&\frac{\partial F(\eta,\tau)}{\partial\eta}\to 1,\ \theta(\eta,\tau)\to 0\ \text{as}\ \eta\to\infty.
\end{aligned} \tag{23}$$

To check the time independent flow solution stability, let us have $\left(F(\eta)=f_0(\eta)\right)f(\eta)=f_0(\eta)$ and $\left(\theta(\eta)=\theta_0(\eta)\right)$ gratifying the BVP (2)–(5), it implements (Merkin [47], Sharma et al. [48] and Weidman et al. [49]).

Let

$$\begin{aligned}
&F(\eta,\tau)=f_0(\eta)+e^{-\varsigma\tau}G(\eta,\tau)\\
&\theta(\eta,\tau)=\theta_0(\eta)+e^{-\varsigma\tau}S(\eta,\tau),
\end{aligned} \tag{24}$$

where ς is a value that is not known (growth and decay distribution) eigenvalue and $G(\eta,\tau)$ and $S(\eta,\tau)$ are too small to be letting $f_0(\eta)$ and $\theta_0(\eta)$, respectively.

Now, plugging Eq. (24) into Eqs. (21) and (22), one infers the subsequent equations:

$$\frac{\left(\frac{\partial^3 f_0}{\partial\eta^3}+e^{-\varsigma\tau}\frac{\partial^3 G}{\partial\eta^3}\right)}{\text{X}_1}+\text{X}_2\left(\left\{f_0+e^{-\varsigma\tau}G\right\}\left\{\frac{\partial^2 f_0}{\partial\eta^2}+e^{-\varsigma\tau}\frac{\partial^2 G}{\partial\eta^2}\right\}+\frac{2m}{m+1}\left(1-\left(\frac{\partial f_0}{\partial\eta}+e^{-\varsigma\tau}\frac{\partial G}{\partial\eta}\right)^2\right)+\varsigma e^{-\varsigma\tau}\frac{\partial G}{\partial\eta}-e^{-\varsigma\tau}\frac{\partial^2 G}{\partial\eta\partial\tau}\right)+\left(\frac{2}{m+1}\right)M\text{X}_3\left(1-\frac{\partial f_0}{\partial\eta}-e^{-\varsigma\tau}\frac{\partial G}{\partial\eta}\right)+\left(\frac{2}{m+1}\right)\lambda_1\cos\left(\frac{\Omega}{2}\right)\text{X}_4\left(\theta_0+e^{-\varsigma\tau}S\right)=0, \tag{25}$$

$$\left\{\frac{\partial^2\theta_0}{\partial\eta^2}+e^{-\varsigma\tau}\frac{\partial^2 S}{\partial\eta^2}\right\}\text{X}_5+\left(\frac{2}{m+1}\right)M\Pr\text{Ec}\left(-e^{-\varsigma\tau}\frac{\partial G}{\partial\eta}-\frac{\partial f_0}{\partial\eta}\right)^2+\Pr\text{X}_6\left(\left\{f_0+e^{-\varsigma\tau}G\right\}\left\{\frac{\partial\theta_0}{\partial\eta}+e^{-\varsigma\tau}\frac{\partial S}{\partial\eta}\right\}-\left(\frac{5m-1}{m+1}\right)\left\{e^{-\varsigma\tau}S+\theta_0\right\}\left\{\frac{\partial f_0}{\partial\eta}+e^{-\varsigma\tau}\frac{\partial G}{\partial\eta}\right\}+\varsigma e^{-\varsigma\tau}S-e^{-\varsigma\tau}\frac{\partial\theta}{\partial\tau}\right)+\frac{\Pr Ec}{\text{X}_1}\left(\frac{\partial^2 f_0}{\partial\eta^2}+e^{-\varsigma\tau}\frac{\partial^2 G}{\partial\eta^2}\right)^2=0 \tag{26}$$

with the conditions are given as:

$$G(0,\tau)=0,\frac{\partial G(0,\tau)}{\partial\eta}=0,S(0,\tau)=0,\ \text{at}\ \eta=0$$
$$\frac{\partial G(\eta,\tau)}{\partial\eta}\to 0,\ S(\eta,\tau)\to 0\ \text{as}\ \eta\to\infty. \tag{27}$$

Following Weidman et al. [49], it is investigated the stable solution for the phenomenon of steady flow $f_0(\eta)$ with heat transfer solution $\theta_0(\eta)$ through site $\tau=0$ and; therefore ,$G=G_0(\eta)$ and $S=S_0(\eta)$ in (25) and (26) to classify early increase/deterioration of the result. Therefore, we explain the subsequent problem linear eigenvalue:

$$\frac{G_0'''}{X_1}+X_2\left(f_0G_0''+Gf_0''-\left(\frac{4m}{m+1}\right)f_0'G_0'+\varsigma G_0'\right)+\left(\frac{2}{m+1}\right)MX_3G_0'$$
$$+\left(\frac{2}{m+1}\right)\lambda_1\cos\left(\frac{\Omega}{2}\right)X_4S_0=0, \tag{28}$$

$$S_0''X_5+\left(\frac{4}{m+1}\right)M\,\mathrm{Pr}\,\mathrm{Ec}f_0'G_0'+\mathrm{Pr}\,X_6\left(f_0S_0'+G_0\theta_0'\right.$$
$$\left.-\left(\frac{5m-1}{m+1}\right)\{\theta_0G_0'+S_0f_0'\}+\varsigma S_0\right)+\frac{2\,\mathrm{Pr}\,\mathrm{Ec}}{X_1}f_0''G_0''=0 \tag{29}$$

with conditions pertaining at boundary is

$$G_0(0)=0,\ S_0(0)=0,G_0'(0)=0,\ \text{at}\ \eta=0$$
$$G_0'\to 0,\ S_0\to 0\ \text{as}\ \eta\to\infty. \tag{30}$$

In this research, the linear eigenvalue equations of IVP (28) and (29) with a new boundary condition (30) is explained by relaxing the condition $G_0(\eta)$ and $S_0(\eta)$. So for here the condition $S_0\to 0$ as $\eta\to\infty$ is relaxed and for unchanged number of ς, Eqs. (28) and (29) in conjunction with the fresh boundary restriction $G_0''(0)=1$ are worked out.

5 Results and Discussion

The system consisting of ODEs (7) and (8) with boundary restriction (9) has been executed numerically through bvp4c solver. The analysis of graphical results of the physical parameters like hybrid nanoparticles (ϕ_1,ϕ_2), mixed convective parameter (λ_1), Eckert number (Ec), magnetic parameter (M) and shrinking/ stretching parameter (λ) are precisely explored on the temperature and velocity profiles together with the heat transfer rate and friction factor in Figs. 2, 3, 4, 5, 6, 7, 8, 9, 10, 11, 12, 13, 14, 15, 16, 17, 18 and 19. The thermo physical features of hybrid nanofluid are depicted in Table 2. Also, check the accuracy of our result's precision, we compare our outcomes in limiting cases with previously published articles [50, 51] and results displayed a tremendous harmony (see Table 3).

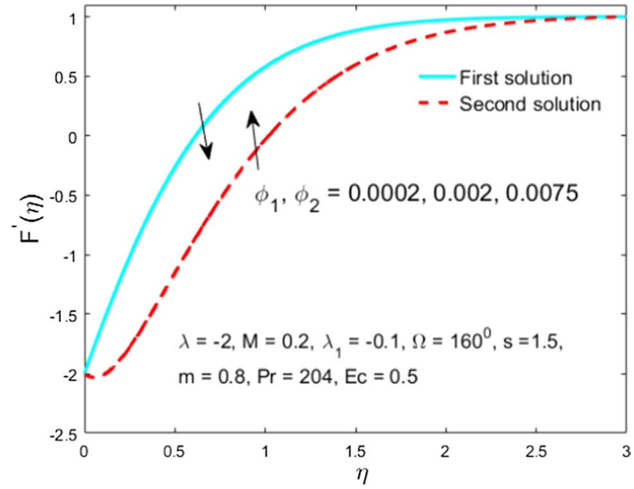

Fig. 2 Influence of ϕ_1,ϕ_2 on $F'(\eta)$

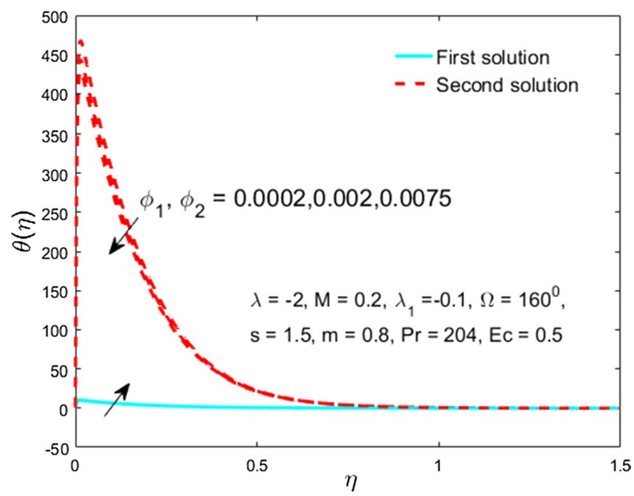

Fig. 3 Influence of ϕ_1,ϕ_2 on $\theta(\eta)$

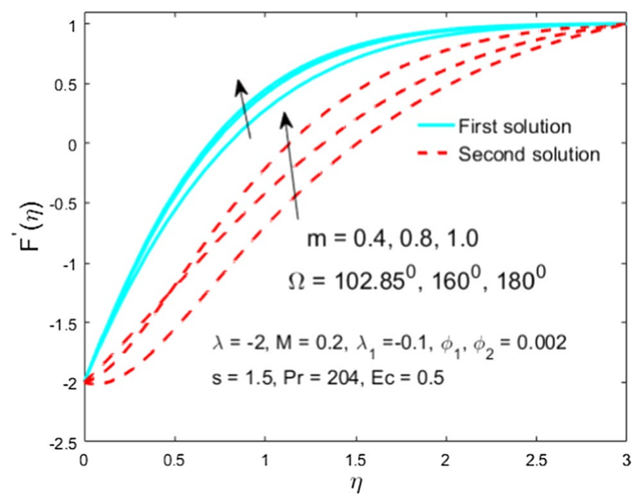

Fig. 4 Influence of m on $F'(\eta)$

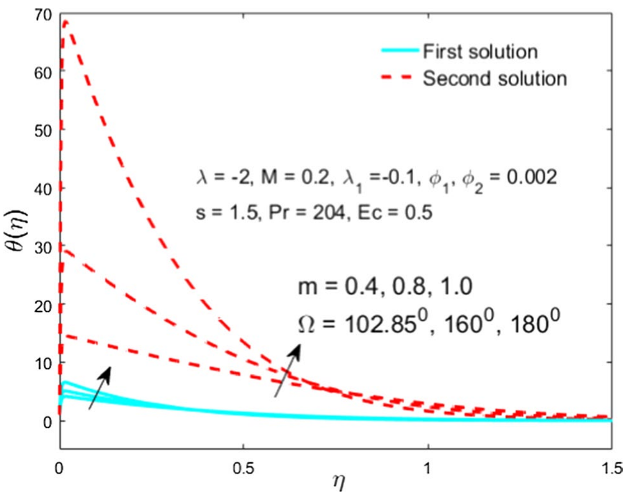

Fig. 5 Influence of m on $\theta(\eta)$

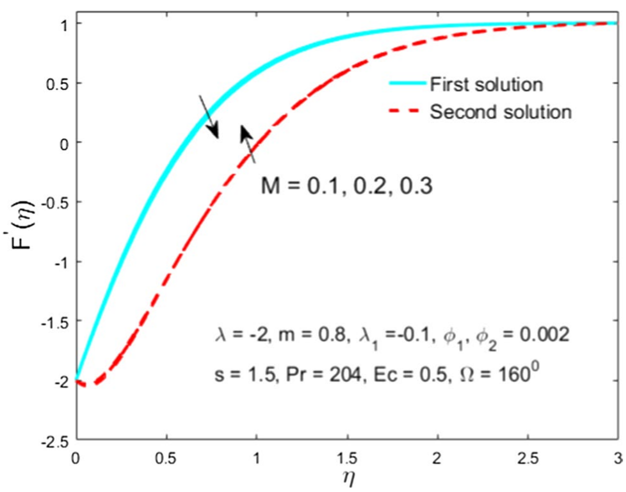

Fig. 6 Influence of M on $F'(\eta)$

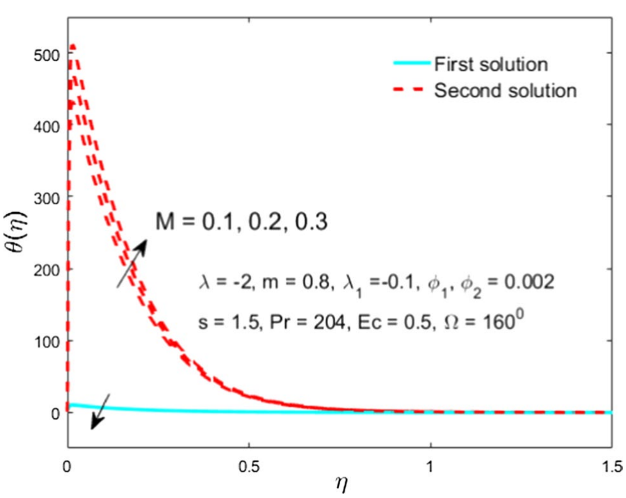

Fig. 7 Influence of M on $\theta(\eta)$

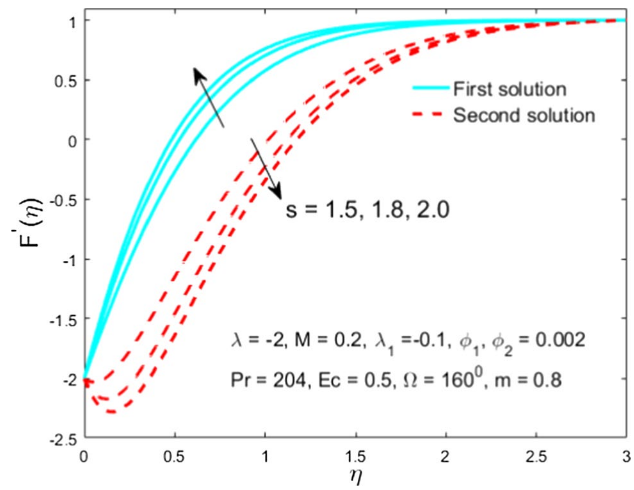

Fig. 8 Influence of s on $F'(\eta)$

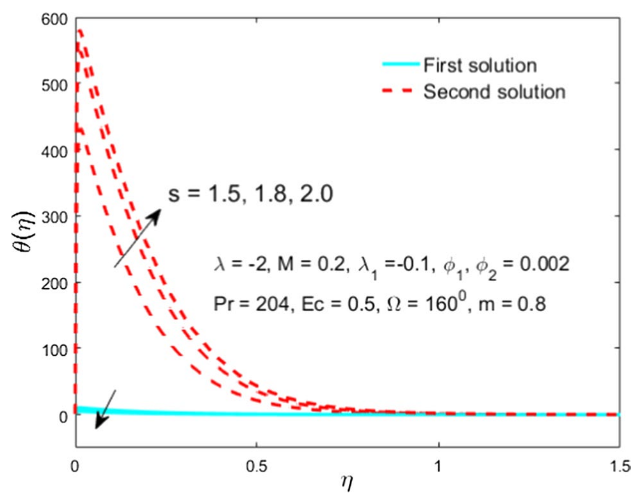

Fig. 9 Influence of s on $\theta(\eta)$

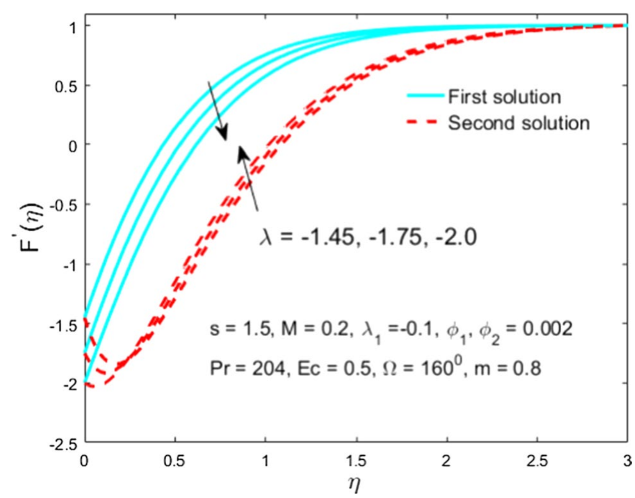

Fig. 10 Influence of λ on $F'(\eta)$

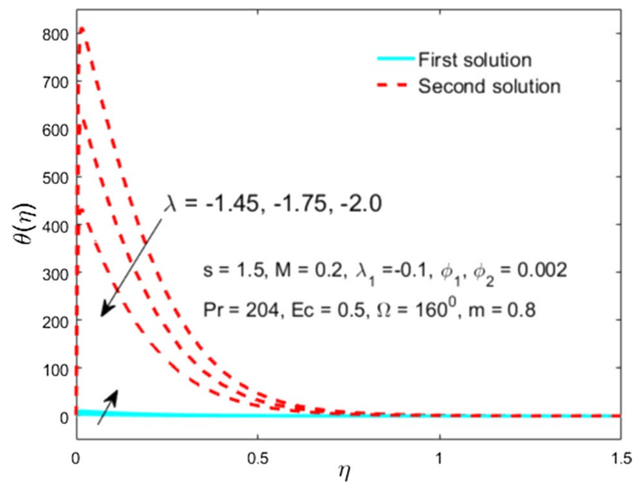

Fig. 11 Effect of λ on $\theta(\eta)$

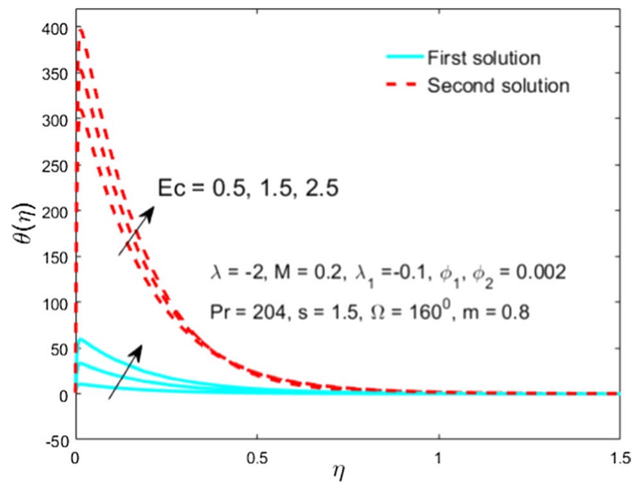

Fig. 14 Effect of Ec on $\theta(\eta)$

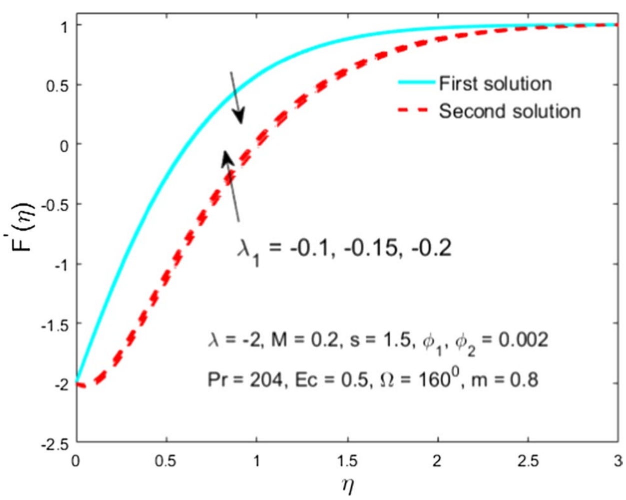

Fig. 12 Influence of λ_1 on $F'(\eta)$

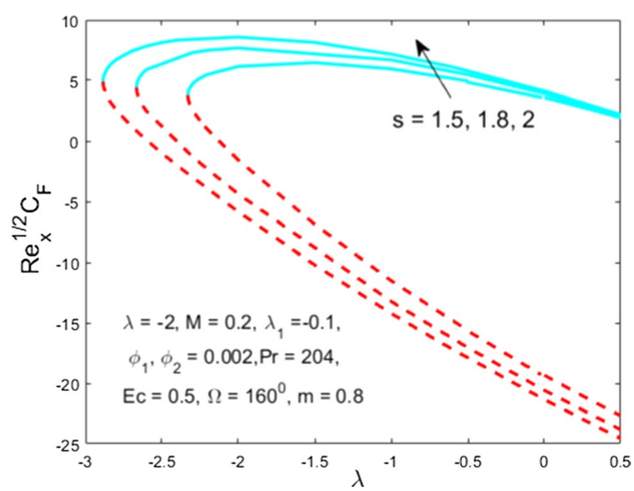

Fig. 15 Impact of s versus λ on $C_F\mathrm{Re}_x^{1/2}$

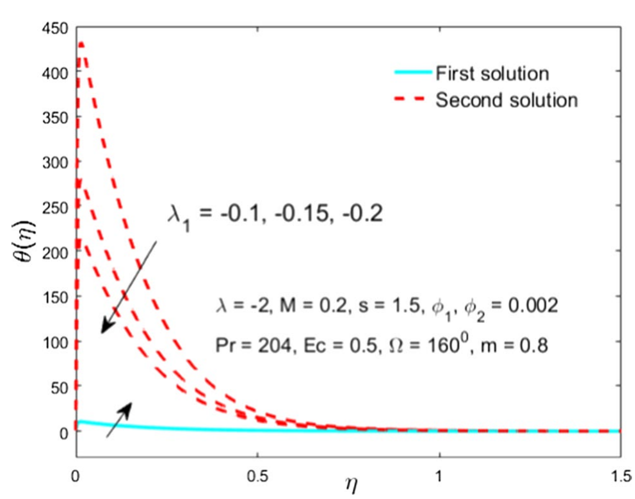

Fig. 13 Effect of λ_1 on $\theta(\eta)$

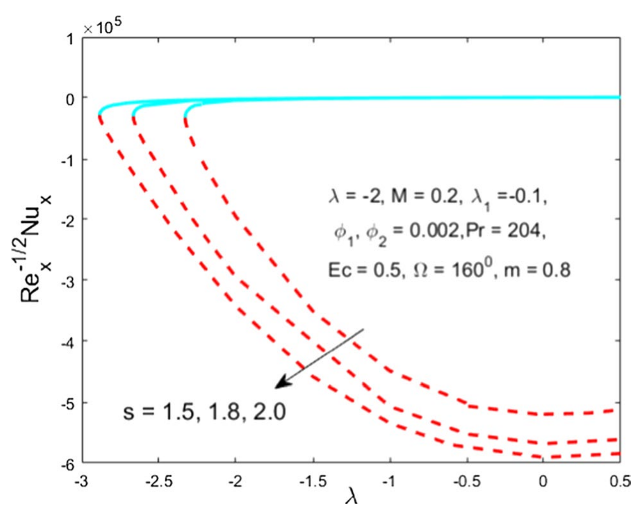

Fig. 16 Impact of s versus λ on $Nu_x\mathrm{Re}_x^{-1/2}$

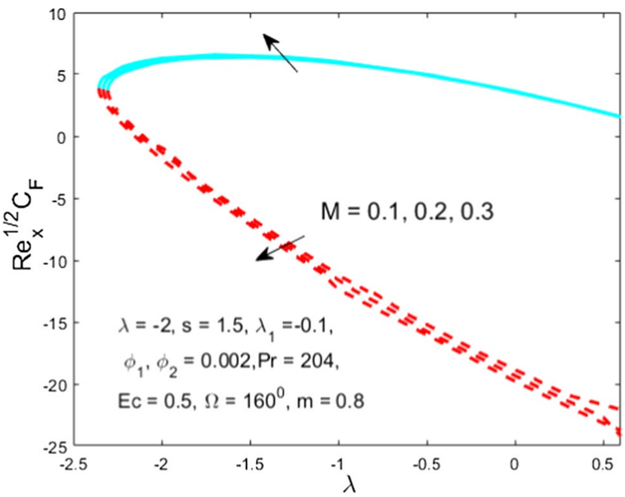

Fig. 17 Impact of M versus λ on $C_F \mathrm{Re}_x^{1/2}$

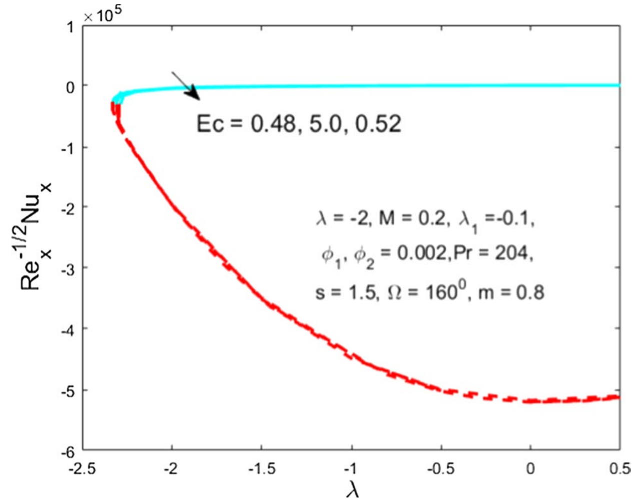

Fig. 19 Influence of Ec versus λ on $\mathrm{Nu}_x \mathrm{Re}_x^{-1/2}$

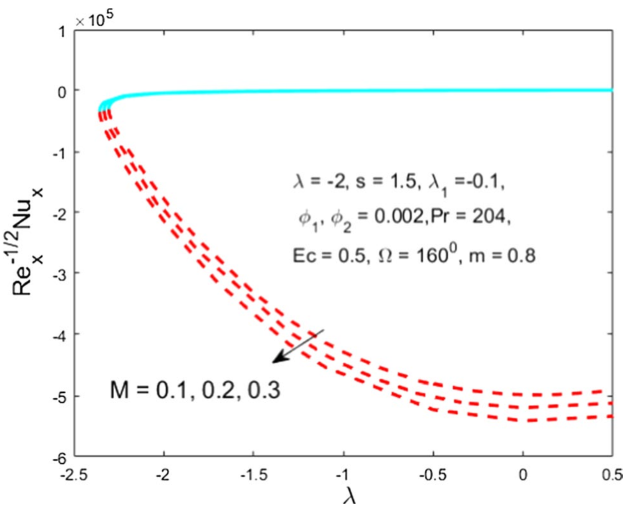

Fig. 18 Impact of M versus λ on $\mathrm{Nu}_x \mathrm{Re}_x^{-1/2}$

Table 2 Thermo physical properties of the base fluid and hybrid nanoparticles [7, 8, 11]

Characteristic properties	Ethylene glycol	SiO_2	MoS_2
ρ [kg/m^3]	1113.5	2650	5060
c_p [J/kg K]	2430	730	397.746
k [W/m K]	0.253	1.5	34.5
β [K^{-1}]	19	42.7	2.8424×10^{-5}
Pr	204		

Table 3 Comparison of $C_{fx}\mathrm{Re}_x^{1/2}$ through different m with $M = 0, \lambda = 0, \phi_1 = \phi_2 = 0$

m	Chamkha et al. [50]	Yacob et al. [51]	Present
− 0.05	0.213484	0.213802	0.2138
0.0	0.332057	0.332206	0.3321
1/3	0.757448	0.757586	0.7574
1.0	1.232588	1.232710	1.2326

5.1 Variation in the Velocity and Temperature Profiles

In Figs. 2 and 3, the impact of alters in increasing amount of hybrid nanoparticles is portrayed on velocity and temperature distribution, respectively. Enhancing hybrid nanoparticles causes a decrease in the fluid velocity (Fig. 2) in the FS, while in the SS, the fluid velocity enhances. In Fig. 3, the temperature distribution augments due to hybrid nanoparticles in the result of the first branch, while in the result of second branch, it declines. Physically, the hybrid nanomaterials scattering augments the thermal energy in the hybrid nanofluid layer which upsurges the temperature. Therefore, the present findings demonstrate that the exploitation of hybrid nanomaterials can help us to develop improved heat circulation in particular heat transfer equipment and can accumulate energy through chemical processes. It is fascinating to perceive that the rise in the profile initially and then asymptotically converge due to the greater value of Prandtl number (Pr = 204). Figures 4 and 5 demonstrate the stimulation of m or Ω on the fluid velocity and fluid temperature, respectively. Furthermore, Fig. 4 describes that the momentum boundary layer decelerate due to wedge angle in first and second results. Figure 5 displays that the temperature of fluid accelerates with augmenting wedge angle in both solutions. The reason behind this that the buoyancy factor owing to thermal diffusion declines due to cos $\Omega/2$ and thus the driving force of the nanoliquid declines and consequently, the temperature enhances. Growing the inclination angle crafts it difficult for the fluid to move along the surface of the wedge and causes it to grow to be warmer due to nanoliquid density is greater. The decline of nanofluid velocity and temperature distribution in the FS by enhancing the magnetic parameter is illustrated in Figs. 6 and 7, respectively, whilst, the opposite trend are captured in the second solution. Physically, the creation of Lorentz force through the augment in the magnetic constraint caused the retardation to flow and declined the temperature and velocity of nanoliquid. The mass suction impact on the profiles of temperature and velocity is inspected in Figs. 9 and 8, respectively. Figure 8 elucidates that the velocity boosts up due to suction in the FS and failures in the SS. Whereas, the temperature of hybrid nanoliquid declines in the FS and augments in the SS as shown in Fig. 9. Physically, the animated liquid is pressed towards a convective wedge wall where the forces of buoyancy can proceed to delay the liquid because of the greater impact of hybrid nanofluid viscosity. Figures 10 and 11 are drawn to see the stretching/shrinking impact on the profiles of velocity and temperature. However, Figs. 10 and 11 reveal that the velocity of nanofluid declines and temperature augments due to stretching/shrinking parameter in the FS, whilst the opposing conduct is analyzed for the second solution. These figures confirm that the broad boundary constraints of the field (9) are met asymptotically, which strengthens the numerical results obtained for the bvp (7) and (8). In addition, it is apparent that profile of velocity boundary-layer develops to be thicker and thicker for the FS as compared to the SS, while the opposite behavior is monitored for the thermal boundary-layer. Figures 12 and 13 are ready to watch the impact of mixed convective parameter on velocity and temperature profiles. In fact, the mixed convective parameter is a combination of buoyancy and viscosity forces. The contrary connection between viscous forces and λ which declines the nanofluid velocity (Fig. 12) and enhance the temperature (Fig. 13) in the branch of FS, whilst the change behavior is scrutinized in the branch of SS. The temperature of the hybrid nanoliquid within the boundary-layer augments with growing Eckert number as depicted in Fig. 14 in the both solutions. Physically, due to rising the liquid friction amid the neighboring layers of liquid rises which consecutively change the kinetic energy into heat energy, and therefore, the liquid temperature goes up.

5.2 Variation in the Skin Friction and the Nusselt Number

Figures 15 and 16 highlight the deviation of the skin factor and the Nusselt number verses parameter λ for different s. It is spotlighted here to investigate the existence of the multiple solutions for shrinking wedge λ up to a certain domain of parameter. Also, these multiple results are acknowledged as the FS (the upper branch) and the SS (the lower branch). The FS is symbolized through solid line and the SS is confined by dotted lines. Since our investigation, it is pragmatic that it can attain the results up to a certain range of λ. In addition, a hurrying drift is monitored for the skin friction factor of the FS, whilst devaluation for the SS is scrutinized with the superior strength of suction as shown in Fig. 15. Also, the diagram in Fig. 16 verifies the aforementioned restriction on λ of existence of dual solutions. It is apparent from this graph that the heat transfer declines for the both solutions by enhancing the suction parameter. Thus more than one solution is obtained for both the heated surface and as well as for the cooled surface up to a certain range of varying parameter lambda as seen in the figures while the solid and dotted line are merged at a point in the aforementioned pictures called the critical points and is denoted by $\lambda = \lambda_c$ whose values are (−2.88470, − 2.66586, − 2.32992). Figures 17 and 18 are revealed to monitor the variation of the skin factor and heat transfer with stretching/shrinking parameter for distinct magnetic number. In these graphs the multiple solutions were found for both phenomena of $\lambda < 0$ and $\lambda > 0$ while the critical points at which the boundary layer is separated and whose count number are (−2.32992, − 2.3350, − 2.35670). Figure 17 explains that the amount of the friction factor augment owing to magnetic number in the first solution and decline in the second solution. Figure 18 reveals that the rate of heat transfer decelerates due to M in both results. The impact of the Eckert number on the heat transfer rate versus λ is shown in Fig. 19. This graph suggests that the values of heat transfer diminish with the augmenting Eckert number in both solutions.

6 Final Remarks

In this work, the impact of magnetic field on mixed convection involving ethylene glycol ($C_2H_6O_2$) based SiO_2–MoS_2 hybrid nanoliquid through a shrinking/stretching wedge is scrutinized. The transmuted ODEs have been examined numerically through bvp4c solver. The essence of the problem is as follows:

- The liquid velocity declines and temperature augments due to hybrid nanoparticle in the result of first branch and contrary trend is seen in the result of the second branch.
- The angle of wedge enhances the profiles of velocity and temperature in both branches of results.
- The magnetic number decelerates the velocity and temperature distribution in the FS, whilst the opposite behavior is noticed in the SS.
- The velocity increases and temperature declines due to the suction in the first solution.

- The momentum and thermal boundary layers enhance due to shrinking parameter in the FS and shrink in the SS.
- Mixed convection parameter decays the velocity and expands the temperature in the FS, whereas the opposite trend is scrutinized in the SS.
- The temperature augments due to Eckert number in both solutions.
- The friction factor increases due to suction and magnetic parameters in the branch of FS, whereas the rate of heat transfer declines.

References

1. Das, P.K.: A review based on the effect and mechanism of thermal conductivity of normal nanofluids and hybrid nanofluids. J. Mol. Liq. **240**, 420–446 (2017)
2. Sarkar, J., Ghosh, P., Adil, A.: A review on hybrid nanofluids: recent research, development and applications. Renew. Sust. Energy Rev. **43**, 164–177 (2015)
3. Sidik, N.A.C., Jamil, M.M., Aziz Japar, W.M.A., Adamu, I.M.: A review on preparation methods, stability and applications of hybrid nanofluids. Renew. Sust. Energy Rev. **80**, 1112–1122 (2017)
4. Senthilaraja, S., Vijayakumar, K., Ganadevi, R.: A comparative study on thermal conductivity of Al_2O_3/water, CuO/water and Al_2O_3–CuO/water nanofluids. Digest J. Nanomat. Biostruc. **10**, 1449–1458 (2015)
5. Toghraie, D., Chaharsoghi, V.A., Afrand, M.: Measurement of thermal conductivity of ZnO–TiO_2/EG hybrid nanofluid Effects of temperature and nanoparticles concentration. J. Therm. Anal. Calorim. **125**, 527–535 (2016)
6. Adriana, M.A.: Hybrid nanofluids based on Al_2O_3, TiO_2 and SiO_2: Numerical evaluation of different approaches. Int. J. Heat Mass Transf. **104**, 852–860 (2017)
7. Maraj, E.N., Iqbal, Z., Azhar, E., Mehmood, Z.: A comprehensive shape factor analysis using transportation of MoS_2-SiO_2/H_2O inside an isothermal semi vertical inverted cone with porous boundary. Res. Phys. **8**, 633–641 (2018)
8. Rostami, M.N., Dinarvand, S., Pop, I.: Dual solutions for mixed convective stagnation-point flow of an aqueous silica-alumina hybrid nanofluid. Chin. J. Phys. **56**(5), 2465–2478 (2018)
9. Mackolil, J., Mahanthesh, B.: Time-dependent nonlinear convective flow and radiative heat transfer of Cu-Al_2O_3-H_2O hybrid nanoliquid with polar particles suspension: a statistical and exact analysis. BioNanoSci. **9**, 937–951 (2019)
10. Shruthy, M., Mahanthesh, M.: Rayleigh-Bénard convection in Casson and hybrid nanofluids: an analytical investigation. J. Nanofluids **8**(1), 222–229 (2019)
11. Ghadikolaei, S.S., Gholinia, M., Hoseini, M.E., Ganji, D.D.: Natural convection MHD flow due to MoS_2–Ag nanoparticles suspended in $C_2H_6O_2$–H_2O hybrid base fluid with thermal radiation. J. Taiwan Inst. Chem. Eng. **97**, 12–23 (2019)
12. Mackolil, J., Mahanthesh, B.: Sensitivity analysis of radiative heat transfer in Casson and nano fluids under diffusion-thermo and heat absorption effects. Eur. Phys. J. Plus **134**, 619 (2019)
13. Mahanthesh, B.: Statistical and exact analysis of MHD flow due to hybrid nanoparticles suspended in $C_2H_6O_2$-H_2O hybrid base fluid. Math. Methods Eng. Appl. Sci. Chapter **8**, 1–44 (2020)
14. Ashlin, T.S., Mahanthesh, B.: Exact solution on non-coaxial rotating and nonlinear convective flow of Cu-Al_2O_3-H_2O hybrid nanofluids over an infinite vertical plate subjected to heat source and radiative heat. J. Nanofluids **8**(4), 781–794 (2019)
15. Thriveni, K., Mahanthesh, B.: Sensitivity analysis of nonlinear radiated heat transport of hybrid nanoliquid in an annulus subjected to the nonlinear Boussinesq approximation. J. Therm. Anal. Cal. (2020). https://doi.org/10.1007/s10973-020-09596-w
16. Falkner, V.M., Skan, S.W.: Some approximate solutions of the boundary layer equations. Phil. Mag. **80**(12), 865–896 (1931)
17. Hartree, D.R.: On an equation occurring in Falkner and Skan's approximate treatment of the equations of the boundary layer. Math. Proc. Cambridge Philos. Soc. **33**(2), 223–239 (1937)
18. Koh, J.C.Y., Hartnett, J.P.: Skin friction and heat transfer for incompressible laminar flow over porous wedges with suction and variable wall temperature. Int. J. Heat Mass Transf. **2**(3), 185–198 (1961)
19. Postelnicu, A., Pop, I.: Falkner-Skan boundary layer flow of a power-law fluid past a stretching wedge. Appl. Math. Comp. **217**, 4359–4368 (2011)
20. Su, X., Zheng, L., Zhang, X., Zhang, J.: MHD mixed convective heat transfer over a permeable stretching wedge with thermal radiation and ohmic heating. Chem. Eng. Sci. **78**, 1–8 (2012)
21. Yang, X.-J., Tenreiro Machado, J.A.: A new fractional operator of variable order: Application in the description of anomalous diffusion. Phys. A: Stat. Mech. Appl. **481**, 276–283 (2017)
22. Yang, X.-J., Gao, F.: A new technology for solving diffusion and heat equations. Thermal Sci. **21**, 133–140 (2017)
23. Zaib, A., Rashidi, M.M., Chamkha, A.J.: Flow of nanofluid containing gyrotactic microorganisms over static wedge in Darcy-Brinkmn porous medium with convective boundary condition. J. Porous Media **21**(10), 911–928 (2018)
24. Yang, X.-J.: General Fractional Derivatives Theory, Methods and Applications, 1st Edition (2019)
25. Yang, X.-J.: Fractional derivatives of constant and variable orders applied to anomalous relaxation models in heat transfer problems. Thermal Sci. **21**(3), 1161–1171 (2019)
26. Yang, X.-J., Gao, F., Ju, Y., Zhou, H.-W.: Fundamental solutions of the general fractional-order diffusion equations. Math. Methods Appl. Sci. **41**(18), 9312–9320 (2018). https://doi.org/10.1002/mma.5341
27. Yang, X.J., Feng, Y.Y., Cattani, C.: Fundamental solutions of anomalous diffusion equations with the decay exponential kernel. Math. Methods Appl. Sci. **42**(11), 4054–4060 (2019). https://doi.org/10.1002/mma.5634
28. Yang, X.-J., Gao, F., Ju, Y.: General Fractional Derivatives with Applications in Viscoelasticity, 1st edition (2020). https://doi.org/10.1016/C2018-0-01749-1
29. Nadeem, S., Ahmad, S., Muhammad, N.: Computational study of Falkner-Skan problem for a static and moving wedge. Sensors Actuat. B: Chem. **263**, 69–76 (2018)
30. Mebarek-Oudina, F., Bessaïh, R.: Numerical simulation of natural convection heat transfer of copper-water nanofluid in a vertical cylindrical annulus with heat sources. Thermophys. Aeromech. **26**(3), 325–334 (2019)
31. Mebarek-Oudina, F.: Convective heat transfer of Titania nanofluids of different base fluids in cylindrical annulus with discrete, heat source. Heat Transfer-Asian Res. **48**(1), 135–147 (2019)
32. Marzougui, S., Mebarek-Oudina, F., Aissa, A., Magherbi, M., Shah, Z., Ramesh, K.: Entropy generation on magneto-convective flow of copper-water nanofluid in a cavity with chamfers. J. Therm. Anal. Calorim. (2020). https://doi.org/10.1007/s10973-020-09662-3
33. Raza, J., Mebarek-Oudina, F., Ram, P., Sharma, S.: MHD flow of non-Newtonian molybdenum disulfide nanofluid in a converging/diverging channel with Rosseland radiation. Defect. Diffus. Forum

401, 92–106 (2020). https://doi.org/10.4028/www.scientific.net/DDF.401.92
34. Mahanthesh, B., Lorenzini, G., Mebarek-Oudina, F., Animasaun, I.L.: Significance of exponential space- and thermal-dependent heat source effects on nanofluid flow due to radially elongated disk with Coriolis and Lorentz forces. J. Therm. Anal. Calorim. (2019). https://doi.org/10.1007/s10973-019-08985-0
35. Raza, J., Mebarek-Oudina, F., Mahanthesh, B.: Magnetohydrodynamic flow of nano Williamson fluid generated by stretching plate with multiple slips. Multidiscipline Modeling Materials Struct. **15**(5), 871–894 (2019)
36. Devi, S.S.U., Devi, S.P.A.: Heat transfer enhancement of Cu−Al_2O_3/water hybrid nanofluid flow over a stretching sheet. J. Niger. Math. Soc. **36**, 419–433 (2017)
37. Hayat, T., Nadeem, S.: Heat transfer enhancement with Ag–CuO/water hybrid nanofluid. Results Phys. **7**, 2317–2324 (2017)
38. Xie, H., Jiang, B., Liu, B., Wang, Q., Xu, J., Pan, F.: An investigation on the tribological performances of the SiO_2-MoS_2 hybrid nanofluids for magnesium alloy-steel contacts. Nanoscale Res. Lett. **11**, 329–336 (2016)
39. Daswita, L., Nazar, R., Ishak, A., Ahmad, R., Pop, I.: Mixed convection boundary layer flow past a wedge with permeable walls. Heat Mass Transf. **46**, 1013–1018 (2010)
40. Ishak, A., Nazar, R., Pop, I.: MHD boundary-layer flow of a micropolar fluid past a wedge with constant wall heat flux. Commun. Nonlinear Sci. Num. Simul. **14**, 109–118 (2009)
41. Raza, J., Mebarek-Oudina, F., Chamkha, A.J.: Magnetohydrodynamic flow of molybdenum disulfide nanofluid in a channel with shape effects. Multidiscip. Model. Mater. Struct. **15**(4), 737–757 (2019)
42. Farhan, M.; Omar, Z.; Mebarek-Oudina, F.; Raza, J.; Shah, Z.; Choudhari, R.V.; Makinde, O.D.: Implementation of one step one hybrid block method on nonlinear equation of the circular sector oscillator. Comput. Math. Model. **31**(1), 116–132 (2020)
43. Hamrelaine, S., Mebarek-Oudina, F., Sari, M.R.: Analysis of MHD Jeffery Hamel flow with suction/injection by homotopy analysis method. J. Adv. Res. Fluid Mech. Therm. Sci. **58**(2), 173–186 (2019)
44. Mebarek-Oudina, F.: Numerical modeling of the hydrodynamic stability in vertical annulus with heat source of different lengths. Eng. Sci. Technol. Int. J. **20**(4), 1324–1333 (2017). https://doi.org/10.1016/j.jestch.2017.08.003
45. Gourari, S., Mebarek-Oudina, F., Hussein, A.K., Kolsi, L., Hassen, W., Younis, O.: Numerical study of natural convection between two coaxial inclined cylinders. Int. J. Heat Technol. **37**(3), 779–786 (2019). https://doi.org/10.18280/ijht.370314
46. Laouira, H., Mebarek-Oudina, F., Hussein, A.K., Kolsi, L., Merah, A., Younis, O.: Heat transfer inside a horizontal channel with an open trapezoidal enclosure subjected to a heat source of different lengths. Heat Transfer-Asian Res. **49**(1), 406–423 (2020)
47. Merkin, J.H.: On dual solutions occurring in mixed convection in a porous medium. J. Eng. Math. **20**(2), 171–179 (1986)
48. Sharma, R., Ishak, A., Pop, I.: Stability analysis of magnetohydrodynamic stagnation-point flow toward a stretching/shrinking sheet. Comp. Fluids **102**, 94–98 (2014)
49. Weidman, P.D., Kubitschek, D.G., Davis, A.M.J.: The effect of transpiration on self-similar boundary layer flow over moving surfaces. Int. J. Eng. Sci. **44**(11–12), 730–737 (2006)
50. Chamkha, A.J., Mujtaba, M., Quadri, A., Issa, C.: Thermal radiation effects on MHD forced convection flow adjacent to a non-isothermal wedge in the presence of a heat source or sink. Heat Mass Transf. **39**, 305–312 (2003)
51. Yacob, N.A., Ishak, A., Pop, I.: Falkner-Skan problem for a static or moving wedge in nanofluids. Int. J. Therm. Sci. **2**(50), 133–139 (2011)